JOURNAL OF GEOPHYSICAL RESEARCH, VOL. 106, NO B5, PAGES 8925-8940, MAY 10, 2001

A two-phase model for compaction and damage 3. Applications to shear localization and plate boundary formation

David Bercovici[1]

Department of Geology and Geophysics, University of Hawaii at Manoa, Honolulu, Hawaii

Yanick Ricard

Laboratoire de Sciences de la Terre, Ecole Normale Supérieure de Lyon, Lyon, France

Gerald Schubert

Department of Earth and Space Sciences, University of California, Los Angeles, California

Abstract. A new two-phase theory employing a nonequilibrium relation between interfacial surface energy, pressure, and viscous deformation [*Bercovici et al.*, this issue] provides a model for damage (void generation and microcracking) and thus a continuum description of weakening, failure, and shear localization. Here we demonstrate applications of the theory to shear localization with simple shear flow calculations in which one phase (the matrix, representing, for example, silicate) is much stronger (more viscous) than the other phase (the fluid). This calculation is motivated as a simple model of plate boundary formation in a shear zone. Even without shear the two phases eventually separate due to gradients in surface tension. However, the influence of shear on phase separation is manifest in several ways. As shear velocity increases, the separation rate of the phases increases, demonstrating a basic feedback mechanism: Accumulation of the fluid phase causes focused weak zones on which shear concentrates, causing more damage and void generation and thus greater accumulation of fluid. Beyond a critical shear velocity, phase separation undergoes intense acceleration and focusing, leading to a "tear localization" in which the porosity becomes nearly singular in space and grows rapidly like a tear or crack. At an even higher value of shear velocity, phase separation is inhibited such that shear localization gives way to defocusing of weak zones suggestive of uniform microcracking and failure throughout the layer. Our two-phase damage theory thus predicts a wide variety of shear localization and failure behavior with a continuum model. Applications of the theory to various fields, such as granular dynamics, metallurgy, and tectonic plate boundary formation are numerous.

1. Introduction

A wide variety of solid materials display strongly nonlinear rheological behavior in that they undergo severe weakening under deformation. Such weakening often leads to a feedback mechanism wherein deformation or shear concentrates on the weak zone (being most easily deformed), causing further weakening, and thus more focusing of shear. This phenomenon is widely referred to as shear localization and is apparent in many field of physics, including, for example, metallurgy [*Lemonds and Needelman*, 1986], rock mechanics [*Poirier*, 1980; *Jin et al.*, 1998, and references therein], granular dynamics [e.g., *Scott*, 1996; *Géminard et al.*, 1999, and references therein], and glaciology [e.g., *Yuen and Schubert*, 1979]. One of the most fundamental manifestations of shear localization arises from the coupling of viscous heating and temperature-dependent viscosity wherein the zone of dissipative heating weakens and thus focuses deformation,

[1]Now at Department of Geology and Geophysics, Yale University, New Haven, Connecticut.

leading to further heating and weakening; this mechanism is thought applicable to problems in metal weakening, glacial surges, and lithosphere dynamics [*Schubert and Turcotte*, 1972; *Yuen and Schubert*, 1979; *Poirier*, 1980; *Balachandar et al.*, 1995; *Bercovici*, 1996; *Thatcher and England*, 1998]. In granular media, localization is due to dilation of the medium leading to effectively weaker rarifed zones that concentrate deformation, which in turn agitates the medium causing further dilation [*Géminard et al.*, 1999, and references therein]; this phenomenon is of potential importance in earthquake dynamics [*Scott*, 1996; *Marone*, 1998; see also *Segall and Rice*, 1995; *Sleep* 1995, 1997]. Another shear localization mechanism arises from the reduction of grain size under stress in solid-state creep mechanisms which have grain-size-dependent viscosities (i.e., grain reduction leads to zones of weakness which concentrate deformation, increasing stress and thus further reducing grain size and enhancing weakening); this mechanism is thought to be a basic ingredient of crustal and lithospheric deformation [*Karato*, 1989; *Jin et al.*, 1998; *Kameyama et al.*, 1997]. Finally, material that undergoes brittle or combined brittle-ductile deformation can, with large strain, experience concentration of microcrack and void populations developing weak bands on which deformation focuses, leading to further cracking, weakening, and invariably shear localization; this phenomenon occurs in the process of dilatant plasticity [*Lemonds and Needelman*, 1986; *Mathur et al.*, 1996] and possibly through much of the crust and lithosphere [*Kohlstedt et al.*, 1995; *Evans and Kohlstedt*, 1995; *Lockner*, 1995; *Regenauer-Lieb*, 1998].

At the largest scale, shear localization is proposed to be crucial for the generation of tectonic plates from a convecting mantle, for which many of the mechanisms listed above are potentially important [*Bercovici*, 1993, 1995a, 1995b, 1996, 1998; *Tackley*, 1998, 2000] (see review by *Bercovici et al.* [2000]). The longevity of plate boundaries [*Gurnis et al.*, 2000], and the inference that much of the lithosphere undergoes combined brittle-ductile behavior [*Kohlstedt et al.*, 1995; Evans and Kohlstedt, 1995] have motivated some [*Bercovici, 1998*; *Tackley*, 1998] to consider that the primary weakening mechanism that leads to plate boundary formation is due to damage, that is, void and microcrack formation. Such damage is assumed to be excited or controlled by the stress state or deformational energy of the system [e.g., *Lemonds and Needleman*, 1986; *Povirk et al.*, 1994; *Lyakhovsky et al.*, 1997; *Bercovici*, 1998]. In many damage treatments the physics of fracture and defect formation is parameterized by an internal structural quantity, e.g., density of defects, that represents the state of damage of the material and is hence often referred to as the "damage" parameter. This quantity is assumed to be an additional thermodynamic state variable [*Ashby and Sammis*, 1990; *Hansen and Schreyer*, 1992; *Lemaitre*, 1992; *Lockner*, 1995; *Lyakhovsky et al.*, 1997] that controls weakening of the material.

In our approach, rather than assume the existence of a structural or damage variable, we employ two-phase physics and interface thermodynamics to incorporate the essential underlying physics of void and microcrack formation into continuum theory. At a most fundamental level the energy involved in damage, or, in particular, the generation of microcracks and voids, is associated with surface free energy created on the boundary between the void and the host material [*Griffith*, 1921; *Jaeger and Cook*, 1979; *Atkinson*, 1987; *Atkinson and Meredith*, 1987]. At a minimum, a material with voids is a two-phase mixture (assuming the host material and the substance filling the voids are both homogeneous matter); hence the surface energy in question is the free energy existing at the interface between phases. In the first paper of this series [*Bercovici et al.*, this issue], (hereinafter referred to as BRS1), we establish a continuum theory to treat two-phase motion accounting for the creation of interfacial surface energy. In the second paper [*Ricard et al.*, this issue], (hereinafter referred to as RBS2), we examin applications of this model to problems of deformation and compaction and to gravity-induced settling when surface tension is significant. In this final paper we examine applications of the BRS1 theory to damage and shear localization. In particular, the theory treats the generation of interfacial surface energy through deformational work, leading to formation of interfacial area by void nucleation and growth. The induced void density or porosity is thus the expression of damage, and regions of high void density are structurally weakened, leading to concentration of deformation, further damage (void generation), weakening, and, invariably, shear localization.

2. Basic Theory

Because BRS1 derived the complete two-phase theory, we only briefly present the governing equations for the purpose of referencing. Subscripts f and m refer to fluid and matrix phases, respectively. All dependent variables are not, in fact, true microscopic quantities but are averaged over the fluid or matrix space within small but not necessarily infinitesimal control volumes (see BRS1). Moreover, all equations are invariant to a permutation of subscripts f and m and, implicitly, a switch of ϕ and $1-\phi$, where ϕ is void or fluid volume fraction, or porosity; this property is called "material invariance" (BRS1).

1. Conservation of mass yields two equations involving transport of the fluid and matrix phases:

$$\frac{\partial \phi}{\partial t} + \boldsymbol{\nabla} \cdot [\phi \mathbf{v}_f] = 0 \tag{1}$$

$$\frac{\partial (1-\phi)}{\partial t} + \boldsymbol{\nabla} \cdot [(1-\phi) \mathbf{v}_m] = 0, \tag{2}$$

where $\mathbf{v}_f$ and and $\mathbf{v}_m$ are the fluid and matrix velocities. Alternatively, (1) and (2) can be combined to yield equations that describe transport of porosity and continuity of average velocity, respectively,

$$\frac{\partial \phi}{\partial t} + \bar{\mathbf{v}} \cdot \boldsymbol{\nabla} \phi = \boldsymbol{\nabla} \cdot [\phi (1-\phi) \Delta \mathbf{v}] \tag{3}$$

$$\boldsymbol{\nabla} \cdot \bar{\mathbf{v}} = 0, \tag{4}$$

where the average and difference of any quantity q are defined as

$$\bar{q} = \phi q_f + (1-\phi) q_m, \qquad \Delta q = q_m - q_f, \tag{5}$$

respectively.

2. The momentum or force balance equations also yield equations describing the dynamics of the two phases:

$$\begin{aligned} 0 = &- \phi \left[\nabla P_f + \rho_f g \hat{\mathbf{z}}\right] + \nabla \cdot \left[\phi \underline{\boldsymbol{\tau}}_f\right] \\ &+ c\Delta\mathbf{v} + \phi \left[\Delta P \nabla\phi + \nabla(\sigma\alpha)\right] \end{aligned} \tag{6}$$

$$\begin{aligned} 0 = &- (1-\phi) \left[\nabla P_m + \rho_m g \hat{\mathbf{z}}\right] + \nabla \cdot \left[(1-\phi) \underline{\boldsymbol{\tau}}_m\right] \\ &- c\Delta\mathbf{v} + (1-\phi) \left[\Delta P \nabla\phi + \nabla(\sigma\alpha)\right], \end{aligned} \tag{7}$$

where P_f and P_m are the fluid and matrix pressures; ρ_f and ρ_m are the fluid and matrix densities, both assumed to be constant;

$$\underline{\boldsymbol{\tau}}_f = \mu_f \left[\nabla \mathbf{v}_f + [\nabla \mathbf{v}_f]^t - \frac{2}{3}(\nabla \cdot \mathbf{v}_f)\underline{\mathbf{I}}\right] \tag{8}$$

$$\underline{\boldsymbol{\tau}}_m = \mu_m \left[\nabla \mathbf{v}_m + [\nabla \mathbf{v}_m]^t - \frac{2}{3}(\nabla \cdot \mathbf{v}_m)\underline{\mathbf{I}}\right] \tag{9}$$

are the fluid and matrix deviatoric stresses, c is a coefficient of proportionality for the viscous interaction forces between the phases, σ is the surface tension which is possibly temperature-dependent,

$$\alpha = \alpha_o \phi^a (1-\phi)^b \tag{10}$$

is the porosity-dependent interfacial area per unit volume in which α_o is a constant with units of m^{-1}, a and b are constants ≤ 1, and $d\alpha/d\phi$ is the average interface curvature (see BRS1 for a discussion of the properties of the interface density). Equations (6) and (7) can be combined into a mixture and difference set:

$$0 = -\nabla \bar{P} + \nabla \cdot \bar{\underline{\boldsymbol{\tau}}} - \bar{\rho} g \hat{\mathbf{z}} + \nabla(\sigma\alpha) \tag{11}$$

$$\begin{aligned} 0 = &- \phi(1-\phi) \left[\nabla \Delta P + \Delta\rho g \hat{\mathbf{z}}\right] \\ &+ \nabla \cdot \left[\phi(1-\phi)\Delta\underline{\boldsymbol{\tau}}\right] - \bar{\underline{\boldsymbol{\tau}}} \cdot \nabla\phi - c\Delta\mathbf{v}. \end{aligned} \tag{12}$$

3. The energy equation is separated into two coupled equations representing (1) the evolution of thermal (entropy-related) energy, and (2) the rate of work done on the interface by pressure, surface tension, and viscous deformational work:

$$\begin{aligned} \overline{\rho c} \frac{\overline{\overline{D}} T}{Dt} &- T \frac{\overline{D}}{Dt}\left(\frac{d\sigma}{dT}\alpha\right) = Q - \nabla \cdot \mathbf{q} \\ &+ B\left(\frac{\overline{D}\phi}{Dt}\right)^2 + (1-f)\Psi \end{aligned} \tag{13}$$

$$\Delta P \frac{\overline{D}\phi}{Dt} + \sigma \frac{\overline{D}\alpha}{Dt} = f\Psi - B\left(\frac{\overline{D}\phi}{Dt}\right)^2, \tag{14}$$

where T is the temperature (assumed the same in both phases), Q is an intrinsic heat source, $\mathbf{q}$ is an energy flux vector (accounting for heat diffusion and possibly energy dispersion; see BRS1), and

$$\Psi = c\Delta v^2 + \phi \nabla \mathbf{v}_f : \underline{\boldsymbol{\tau}}_f + (1-\phi)\nabla \mathbf{v}_m : \underline{\boldsymbol{\tau}}_m \tag{15}$$

(where $\Delta v^2 = \Delta\mathbf{v} \cdot \Delta\mathbf{v}$) is the viscous deformational work, a fraction f of which is partitioned into stored work (in this model stored as interface surface energy) while the remaining part goes toward dissipative heating [*Taylor and Quinney*, 1934; *Chrysochoos and Martin*, 1989]; see BRS1 for a discussion of the partitioning fraction f. The quantity B has units of viscosity, and the term associated with it represents irreversible viscous work done on pores and grains by the pressure difference ΔP during compaction or dilation (see BRS1 and RBS2). Simple micromechanical models (BRS1) suggest that

$$B = K_0 \frac{(\mu_m + \mu_f)}{\phi(1-\phi)}, \tag{16}$$

where K_0 is a dimensionless factor accounting for pore or grain geometry; it is typically $O(1)$ (see BRS1). The average heat capacity per volume of the mixture is

$$\overline{\rho c} = \phi \rho_f c_f + (1-\phi)\rho_m c_m \tag{17}$$

(where c_f and c_m are the heat capacities of the fluid and matrix), and the material derivatives in (13) and (14) are defined as

$$\frac{\overline{D}}{Dt} = \frac{\partial}{\partial t} + \bar{\mathbf{v}} \cdot \nabla \tag{18}$$

$$\frac{\overline{\overline{D}}}{Dt} = \frac{1}{\overline{\rho c}}\left(\phi\rho_f c_f \frac{D_f}{Dt} + (1-\phi)\rho_m c_m \frac{D_m}{Dt}\right) \tag{19}$$

in which

$$\frac{D_f}{Dt} = \frac{\partial}{\partial t} + \mathbf{v}_f \cdot \nabla, \qquad \frac{D_m}{Dt} = \frac{\partial}{\partial t} + \mathbf{v}_m \cdot \nabla. \tag{20}$$

Relation (14) can be considered a nonequilibrium, mixture proxy for the stress jump condition across the interface between phases (see BRS1 for further discussion), given that the interface location and orientation cannot be known in a mixture theory. However, this relation with $f\Psi > 0$ also describes the deposition of deformational work as surface energy; as more deformational work is imposed, more interfacial surface area is created to store the energy, generally leading to growth in void density or porosity. Throughout this paper, for the sake of brevity, we refer to the application of viscous deformational work to the generation of surface energy (i.e., cases with $f > 0$), thus leading to growth in interface area and void density, as "damage", although strictly speaking, this may not be the same definition of damage as used elsewhere [*Ashby and Sammis*, 1990; *Lyakhovsky et al.*, 1997; see *Lemaitre*, 1992; *Hansen and Schreyer*, 1992, and references therein]. We will examine a few simple one-dimensional (1-D), time-dependent scenarios to illustrate the basic physics of shear localization through the damage process as predicted by this theory. Presently, we will assume

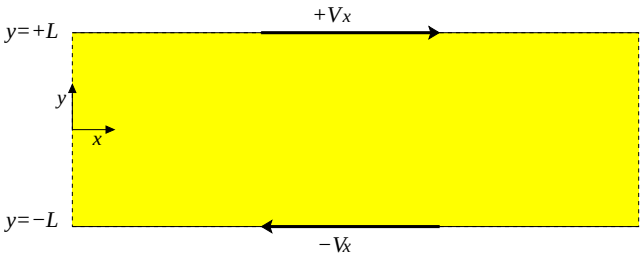

Figure 1. Sketch of model geometry for one-dimensional shear and self-separation calculations. Dimensional variables are shown. After nondimensionalization, $y = \pm L$ is replaced by $y = \pm 100$ and $\pm V_x$ is replaced by $\pm U$.

that σ is constant such that temperature T has no influence on the dynamics. We will consider thermal effects in future papers.

We will first examine the simplest possible physics of unforced phase separation in the absence of damage ($f\Psi \approx 0$), a process hence called "self-separation". Although this problem does not explicitly pertain to damage and shear localization, it is important to examine as a starting point for understanding damage processes.

Last, we will examine the influence of shear and damage or deformational work ($f\Psi > 0$), which leads to highly accelerated separation of the phases, resulting in weakening and enhanced shear over concentrations of the fluid phase and thus a runaway shear localization, termed a "tear localization," suggestive of crack formation.

3. General One-Dimensional Equations

Our model layer is infinitely long in the x direction and is $2L$ wide, going from $y = -L$ to $+L$ (Figure 1). The boundaries are impermeable and no slip and move in the x direction with equal and opposite velocities of magnitude V_x; thus at $y = \pm L$, $v_{m_x} = v_{f_x} = \pm V_x$ and $v_{m_y} = v_{f_y} = 0$. (For self-separation the x component of the boundary velocities is irrelevant.) In some instances, we consider an infinite domain ($L \to \infty$) for which these boundary conditions require some adjustment; these cases will be discussed as needed. We specify that all dependent variables depend only on y and time t.

Because the system is one-dimensional and the boundaries at $y = \pm L$ are rigid (i.e., $v_{m_y} = v_{f_y} = 0$ at the boundaries, or as $y \to \pm\infty$), the continuity equation (4) becomes $\phi v_{f_y} + (1-\phi) v_{m_y} = 0$; if $\phi \neq 0$, then we obtain

$$v_{f_y} = -\frac{1-\phi}{\phi} v_{m_y}, \qquad \Delta v_y = v_{m_y}/\phi\,. \tag{21}$$

Mass conservation (2) (or (3)) yields

$$\frac{\partial \phi}{\partial t} = \frac{\partial}{\partial y}[(1-\phi) v_{m_y}]. \tag{22}$$

Our layer is assumed to be in the horizontal x-y plane such that gravity does not appear in the relevant force equations. We also assume that $\mu_f \ll \mu_m$ and that the fluid macroscopic stresses are negligible relative to other fluid forces; thus we neglect $\underline{\tau}_f$ but retain interface force terms proportional to $c\Delta\mathbf{v}$. Given the formula for c in the limit $\mu_f \ll \mu_m$ [see BRS1; *McKenzie*, 1984; *Spiegelman*, 1993a, 1993b, 1993c], we obtain

$$c = \frac{\mu_f \phi^2}{k_o \phi^n}, \tag{23}$$

where k_o is a reference permeability; adopting the common and simplifying assumption that $n = 2$ (which is really only valid for small porosities), $c = \mu_f / k_o$ is a constant.

With the above assumptions the x component of the fluid force equation (6) yields $c\Delta v_x = 0$, which implies that $v_{f_x} = v_{m_x}$ throughout the medium. The x component of the matrix force equation (7) becomes

$$0 = \mu_m \frac{\partial}{\partial y}\left[(1-\phi)\frac{\partial v_{m_x}}{\partial y}\right]. \tag{24}$$

The only equation necessary to describe the force balance in the y direction is (12), which, with the above assumptions, becomes

$$0 = -\phi(1-\phi)\frac{\partial \Delta P}{\partial y} + \frac{4}{3}\mu_m \phi \frac{\partial}{\partial y}\left[(1-\phi)\frac{\partial v_{m_y}}{\partial y}\right] - c\frac{v_{m_y}}{\phi}. \tag{25}$$

Assuming that σ is constant, the final necessary equation is (14), which, with our assumptions so far, becomes

$$\left(\Delta P + \sigma \frac{d\alpha}{d\phi} + K_0 \frac{\mu_m}{\phi(1-\phi)}\frac{\partial \phi}{\partial t}\right)\frac{\partial \phi}{\partial t} = f\Psi, \tag{26}$$

where

$$\Psi = c\frac{v_{m_y}^2}{\phi^2} + \mu_m(1-\phi)\left[\left(\frac{\partial v_{m_x}}{\partial y}\right)^2 + \frac{4}{3}\left(\frac{\partial v_{m_y}}{\partial y}\right)^2\right]. \tag{27}$$

We must also consider the special situation of $\phi = 0$ (since (21)–(27) are valid for $0 < \phi < 1$). In this case, and given our assumptions so far, (4) becomes $\Delta v_y \partial\phi/\partial y = \partial v_{m_y}/\partial y$. However, since $\phi = 0$ is the minimum value of ϕ, $\partial\phi/\partial y = 0$ when $\phi = 0$, and thus $\partial v_{m_y}/\partial y = 0$; also, with the rigid boundaries, $v_{m_y} = 0$ when $\phi = 0$. These two constraints on v_{m_y} lead to $\partial\phi/\partial t = 0$ (from (22)). These relations would then replace (22) and (25) as the relevant equations for the case $\phi = 0$. Similar conditions exist for the case $\phi = 1$, assuming that our basic approximations (e.g., that $\underline{\tau}_f$ is negligible) are applicable in this limit.

To nondimensionalize the governing equations, we use a length scale R that is characteristic of the width of the fluid zone upon complete phase separation (or the sum of all fluid zone widths if there are multiple regions of phase separation). We do not choose the layer width L as our length scale since we consider some cases involving infinite domains, i.e., $L \to \infty$; in these situations we assume that a finite amount of fluid is present and thus the width of the zone of separated fluid is finite. We also do not use the compaction length $\sqrt{4\mu_m/(3c)}$ (see RBS2) as our length scale

since we wish to vary the resistance to Darcy flow characterized by the coefficient c. We thus assign R to be characteristic of the half width of the fluid zone and therefore consider two possible cases:

1. If the layer is finite, then the half width of the fluid zone is

$$\frac{1}{2}\int_{-L}^{+L}\phi dy = L\langle\phi\rangle, \tag{28}$$

where $\langle\phi\rangle$ is the volume-averaged porosity. Rather than prescribe $\langle\phi\rangle$, we assume it is typically of order 10^{-2} and that the characteristic scale for the half width of the fluid zone is $R = 10^{-2}L$. This length scale will be applied to most of our cases.

2. When the layer is infinite ($L \to \infty$), we must alter the definition of R slightly. In this situation we assume that $\phi(y)$ is well behaved as $y \to \pm\infty$, that is, it decays over a finite width $\tilde{\delta}$ which we refer to as the scale width of ϕ. The scale width $\tilde{\delta}$ can change in time as the peak porosity grows or decays. The half width of the fluid zone is then

$$\frac{1}{2}\int_{-\infty}^{+\infty}\phi dy = \eta\tilde{\delta}_{\min}, \tag{29}$$

where η is a dimensionless constant ≈ 1 (and determined by the shape of the function $\phi(y)$; see section 4.3.1 in which one obtains $\eta = \pi/2$), while $\tilde{\delta}_{\min}$ is the minimum allowable porosity scale width obtained when the peak porosity reaches 1; $\tilde{\delta}_{\min}$ is therefore approximately equal to the half width of the fluid zone. Thus, in this situation we choose $R = \tilde{\delta}_{\min}$.

In both of the above cases, the length scale R is characteristic of the fluid zone half width, and thus all model situations, whether the domains are finite or infinite, are comparably scaled.

With the nondimensionalization of distance by R, time by $4\mu_m/(3\sigma\alpha_o)$, and pressure by $\sigma\alpha_o$, the governing equations become

$$\frac{\partial\phi}{\partial t} = \frac{\partial}{\partial y}[(1-\phi)w], \tag{30}$$

$$0 = \frac{\partial}{\partial y}\left[(1-\phi)\frac{\partial u}{\partial y}\right], \tag{31}$$

$$0 = -\phi(1-\phi)\frac{\partial\Delta\Pi}{\partial y} + \phi\frac{\partial}{\partial y}\left[(1-\phi)\frac{\partial w}{\partial y}\right] - \lambda\frac{w}{\phi}, \tag{32}$$

$$\left(\Delta\Pi + \frac{d\alpha'}{d\phi} + \frac{\kappa}{\phi(1-\phi)}\frac{\partial\phi}{\partial t}\right)\frac{\partial\phi}{\partial t} = f\Psi', \tag{33}$$

where

$$(u,w) = \left[\frac{4\mu_m}{3R\sigma\alpha_o}\right](v_{m_x}, v_{m_y}) \tag{34}$$

are the dimensionless matrix velocities,

$$\Delta\Pi = \frac{\Delta P}{\sigma\alpha_o} \tag{35}$$

is the dimensionless pressure difference,

$$\Psi' = \lambda\frac{w^2}{\phi^2} + (1-\phi)\left[\frac{3}{4}\left(\frac{\partial u}{\partial y}\right)^2 + \left(\frac{\partial w}{\partial y}\right)^2\right] \tag{36}$$

Table 1. Key Dimensionless Variables and Parameters for the One-Dimensional Model

Variable or Parameter	Description	Defining Equation
ϕ	porosity	(30)
u	x (along-channel) velocity	(31),(34)
w	y (cross-channel) velocity	(32),(34)
$\Delta\Pi$	matrix-fluid pressure difference	(33), (35), (59)
Ψ'	rate of deformational work	(36)
$\alpha'(\phi)$	interface area per unit volume ($d\alpha'/d\phi$ equals sum of interface curvatures)	(37)
$G(\phi)$	coefficient for surface tension force (proportional to $-d^2\alpha'/d\phi^2$)	(43)
$\Phi_0(t)$	peak ϕ (for amplitude analysis)	(47)
$W_0(t)$	peak w (for amplitude analysis)	(50)
$\delta(t) = 1/\Phi_0(t)$	porosity anomaly half width (for amplitude analysis	(47),(49)
a, b	interface area and curvature exponents (control dependence of α' on ϕ	(37)
λ	Darcy resistance coefficient (related to compaction length)	(39)
κ	coefficient for viscous resistance to compaction/dilation	(16),(38)
U	imposed shear velocity in x direction	(40)
f	partitioning fraction of deformational work applied to interface	(33), (58)
f^*	maximum value of f	(58)
γ	controls dependence of f on $\partial\phi/\partial t$	(58)
ν	proportional to f^*U^2/γ (scaling parameter controlling the dependence of damage on U, f^* and γ)	(62)

$$\alpha' = \alpha/\alpha_o = \phi^a(1-\phi)^b, \tag{37}$$

$$\kappa = 3K_0/4, \tag{38}$$

$$\lambda = \frac{3cR^2}{4\mu_m}, \tag{39}$$

which contains information about the compaction length $\sqrt{4\mu_m/(3c)}$ [see RBS2; *McKenzie*, 1984]; see Table 1 for summary of dimensionless variables and parameters.

For finite layers in which $R = 10^{-2}L$, the dimensionless domain is given by $-100 \le y \le 100$, and the boundary

conditions on velocity are now

$$w = 0, \qquad u = \pm U = \pm \frac{4\mu_m V_x}{3R\sigma\alpha_o} \tag{40}$$

at $y = \pm 100$. For infinite layers ($L = \infty$ and $R = \tilde{\delta}_{\min}$) we obtain $-\infty \leq y \leq \infty$ and $w \to 0$ as $y \to \pm\infty$; the boundary conditions on u require slightly more discussion, which we defer to section 5.3.1.

4. Self-Separation

In this paper, shear localization occurs because with imposed deformation the fluid and matrix separate from an initially homogeneous mixture and the concentration of fluid causes a weak zone on which shear focuses. However, even without imposed shear, the phases undergo unforced self-separation in the presence of surface tension and porosity gradients. For example, a positive porosity anomaly has a smaller average interface curvature $d\alpha/d\phi$, and thus a smaller surface tension force acting on the fluid, than in surrounding areas. This causes a fluid pressure low in the porosity anomaly, which thereby attracts more fluid, causing inflation of the porosity anomaly and self-separation. The self-separation effect is always present, and in many ways, shear and damage merely act to accelerate this self-separation. It is therefore important to elucidate the physics of simple self-separation. However, it should be understood that the self-separation instability described herein is neither directly related to, nor offsets, the stabilization of crack and bubble nucleation by surface tension; in the former case the instability essentially involves coalescence of preexisting fluid bubbles (or matrix grains) as occurs in oil and water (sans gravity), while the latter reflects the additional work necessary to grow or nucleate new bubbles or cracks because of surface tension (this effect is explicitly in the theory through (14)). Different aspects of self-separation effect are also discussed in RBS2 as pertinent for percolation and compaction problems.

4.1. Specific Equations

For simple self-separation we assume that damage or deformational work on the interface is negligible compared to surface tension and pressure work, ($f\Psi' \approx 0$), in which case, (33) becomes

$$\Delta\Pi = -\frac{d\alpha'}{d\phi} - \frac{\kappa}{\phi(1-\phi)}\frac{\partial\phi}{\partial t} \tag{41}$$

(assuming that (33) holds for all $\partial\phi/\partial t$); note that in the limit of static equilibrium $\partial\phi/\partial t \to 0$, (41) recovers the Laplace equilibrium condition for surface tension $\Delta\Pi = -d\alpha'/d\phi$, where $d\alpha'/d\phi$ represents interface curvature. Since $f\Psi'$ is neglected, the x component of velocity u has no influence on the dynamics of separation and thus there is no external forcing of phase separation; it is thus unnecessary to solve (31), and all solutions are therefore independent of the boundary velocity U.

Apart from the mass conservation equation (30), the only relevant equation is obtained by using the force balance (41) to eliminate $\Delta\Pi$ from (32) (and multiplying the resulting equation by $\phi(1-\phi)$) to yield

$$\begin{aligned} 0 = &- G(\phi)\frac{\partial\phi}{\partial y} + \phi^2(1-\phi)\frac{\partial}{\partial y}\left[(1-\phi)\frac{\partial w}{\partial y}\right] \\ &+ \kappa\phi^2(1-\phi)^2\frac{\partial}{\partial y}\left[\frac{1}{\phi(1-\phi)}\frac{\partial\phi}{\partial t}\right] - \lambda(1-\phi)w, \end{aligned} \tag{42}$$

where

$$G(\phi) = \phi^a(1-\phi)^b\left\{a(1-a)+(a+b-1)[2a-(a+b)\phi]\phi\right\}. \tag{43}$$

As noted by RBS2, the quantity $G(\phi)$ is positive for all a, b, and ϕ, given $0 \leq a, b, \phi \leq 1$.

4.2. Linear Stability Analysis

We next examine the initiation of self-separation from an infinitesimal perturbation. We prescribe the medium to be finite ($-100 \leq y \leq 100$) and to have a static basic state ($w = w_0 = 0$) with constant porosity ϕ_0. Including perturbations to this basic state, we write porosity and velocity as $\phi = \phi_0 + \epsilon\phi_1$ and $w = \epsilon w_1$, respectively, where $\epsilon \ll 1$. Thus (30) and (42) become, to order ϵ^1,

$$\frac{\partial\phi_1}{\partial t} = (1-\phi_0)\frac{\partial w_1}{\partial y} \tag{44}$$

$$0 = -G_0\frac{\partial\phi_1}{\partial y} + \phi_0(\kappa+\phi_0)(1-\phi_0)^2\frac{\partial^2 w_1}{\partial y^2} - \lambda(1-\phi_0)w_1, \tag{45}$$

where $G_0 = G(\phi_0)$, and we have used (30) to eliminate $\partial\phi/\partial t$ from (42). Assuming both ϕ_1 and w_1 go as e^{iky+st}, we arrive at a dispersion relation for the growth rate

$$s = \frac{G_0 k^2}{\phi_0(\kappa+\phi_0)(1-\phi_0)k^2 + \lambda}\ . \tag{46}$$

Given that G_0 is greater than 0, the growth rate $s > 0$, and thus all perturbations are unstable. However, there is no one maximum growth rate s at a finite value of k and thus no least stable mode. Nevertheless, there is some scale selection because the function $s(k)$ acts as a high-pass filter; that is, all modes with $k \gg \sqrt{\lambda/[\phi_0(\kappa+\phi_0)(1-\phi_0)]}$ are preferred since they grow at the maximum growth rate $G_0/[\phi_0(\kappa+\phi_0)(1-\phi_0)]$, while modes with $k \leq \sqrt{\lambda/[\phi_0(\kappa+\phi_0)(1-\phi_0)]}$ grow much more slowly and will be effectively "filtered out." Thus, if $\lambda \ll \phi_0(\kappa+\phi_0)(1-\phi_0)$, essentially all modes will grow equally fast at the maximum rate; in this case, there is effectively no resistance to Darcy flow and fluid can be drawn from any distance (i.e., the compaction length is effectively infinite). An increase in the value of λ causes longer-wavelength (smaller k) perturbations to be filtered out relative to shorter-wavelength features; this process reflects the fact that the greater resistance to Darcy flow precludes migration of fluid over large distances such that fluid is only drawn from within a finite compaction length $\sqrt{4\mu_m/(3c)}$. (See RBS2 for further details about cases with finite λ.)

4.3. Nonlinear Solutions

In this section we seek nonlinear solutions to our one-dimensional system of self-separation. We first examine some simple analytical relationships for the amplitude of nonlinear solutions and then investigate some numerical solutions to the full equations.

4.3.1. Amplitude analysis. An approximate solution for the growth in amplitude of a porosity anomaly can be obtained by assuming forms of solutions with the proper symmetry about the midplane $y = 0$. In particular, If ϕ is an even function of y and maximum at $y = 0$, then self-separation will occur such that matrix material flows away from the plane at $y = 0$, while fluid flows toward it; in this case, w would be an odd function of y (positive for $y > 0$ and negative for $y < 0$). We assume that the porosity anomaly varies in y only over the (dimensionless) scale width δ with a self-similar shape; for simplicity, we assume that

$$\phi = \frac{\Phi_o(t)}{1 + y^2/\delta^2(t)} \quad , \tag{47}$$

although other symmetric functions would also suffice. Since we prescribe $\phi(y)$ to be self-similar, varying over only one length scale δ, we must preclude the influence of other length scales. To this end, we assume an infinite domain, i.e., $-\infty \leq y \leq \infty$, and an infinite compaction length, i.e., $\lambda \approx 0$, such that no additional scale selection occurs at the onset of the self-separation instability (see section 4.2 on linear stability). The scale width δ is not constant; that is, as the porosity amplitude Φ_o grows, δ must shrink in order to conserve mass; indeed, by fluid mass conservation,

$$\int_{-\infty}^{+\infty} \phi(y)dy = \pi\Phi_o(t)\delta(t) = \text{const.} \tag{48}$$

The maximum allowable value of Φ_o is 1, at which point the minimum δ obtained is also 1 (having, with our infinite domain, nondimensionalized lengths by the dimensional minimum scale-width $\tilde{\delta}_{\text{min}}$; see section 3). Therefore, by (48), $\Phi_o(t)\delta(t) = 1$, or

$$\delta(t) = \frac{1}{\Phi_o(t)}. \tag{49}$$

We assume that the dependence of w on y/δ also follows a self-similar shape that vanishes at $y = \pm\infty$; however, the shape of w may be slightly more complex than that of ϕ. In the simplest example, if the fluid momentum equation reduced to Darcy's law (corresponding to the assumptions of $\mu_f \ll \mu_m$ and weak compaction/dilation, $\partial\phi/\partial t \ll 1$), then in our 1-D system, $w \sim \phi^2\partial\Pi_f/\partial y$, where Π_f is the dimensionless fluid pressure. If we crudely assume that the fluid pressure anomaly mirrors the porosity anomaly (i.e., $\Pi_f \sim (1 + y^2/\delta^2)^{-1}$), then we can write

$$w = \frac{W_o y/\delta}{(1 + y^2/\delta^2)^4} \quad , \tag{50}$$

suggesting that $|w|$ decays with $|y|$ more rapidly than does ϕ. With signficant compaction/dilation (nonnegligible $\partial\phi/\partial t$) the relation for w is only slightly more complicated. Thus for the sake of simplicity, we continue to employ (50).

If we substitute (47) and (50) into (30) and into $\partial/\partial y$ of (42) (where the y derivative is taken so that the terms in (42) are even about $y = 0$) and evaluate the resulting terms at the centerline $y = 0$, we obtain

$$\frac{\partial\Phi_o}{\partial t} = \Phi_o(1 - \Phi_o)W_o \tag{51}$$

$$0 = G(\Phi_o) - \Phi_o(1 - \Phi_o)\Big[\Phi_o(12 - 13\Phi_o) + \kappa(11 - 13\Phi_o)\Big]W_o, \tag{52}$$

where we have used $\delta = 1/\Phi_o$. If other self-similar trial functions are chosen for ϕ and w, then instead of the factors $12 - 13\Phi_o$ or $11 - 13\Phi_o$ in (52), one obtains terms of the form $M - N\Phi_o$ in which $M \approx N \sim O(10)$. Therefore, given the approximate nature of the presumed shapes of ϕ and w, we assume for simplicity that the distinction between $12 - 13\Phi_o$ (or $11 - 13\Phi_o$) and $12(1 - \Phi_o)$ is not meaningful; thus we write

$$W_o = \frac{G(\Phi_o)}{12\Phi_o(\kappa + \Phi_o)(1 - \Phi_o)^2}, \tag{53}$$

which, when combined with (51), yields a single differential equation for Φ_o that has the implicit solution

$$t(\Phi_o) = 12\int \frac{(\kappa + \Phi_o)(1 - \Phi_o)d\Phi_o}{G(\Phi_o)}. \tag{54}$$

Analytic solutions to this integral exist for only a few select a and $b = a$:

1. If $a = b = 0$, the surface energy is independent of ϕ and there will be no self-separation. In this case, $G(\Phi_o) = 0$, and the time to cause complete separation (i.e., to go from $\Phi_o \approx 0$ to $\Phi_o = 1$) is infinite.

2. If $a = b = 1$, we obtain an implicit solution

$$t - t_o = 6\left[(\kappa + 1)\ln\left(\frac{\Phi_o}{1 - \Phi_o}\right) - \frac{\kappa}{\Phi_o},\right] \tag{55}$$

where t_o is an integration constant. Although separation does occur, the time to cause complete separation (i.e., to go entirely from $\Phi_o \approx 0$ to $\Phi_o = 1$) is infinite also. This asymptotic separation can be interpreted to occur because with $a = b = 1$ the interface curvature $d\alpha/d\phi$ is finite even when $\phi = 0$, while the resistance to Darcy flow through the matrix becomes infinite (i.e., permeability $k_o\phi^n$ vanishes) as $\phi \to 0$. Thus, as pores collapse, the surface tension driving force remains finite, while resistance to draining fluid from the pores becomes infinite, implying that the pores cannot be entirely collapsed.

3. When a and b are neither 0 nor 1, the interface curvature goes to infinity as $\phi \to 0$. Thus even as the resistance to Darcy flow becomes infinite as ϕ approaches 0, the driving force behind draining the pores, i.e., the surface tension, also becomes infinite. In effect, the surface tension can

completely pinch the pores closed, and thus the pores can be drained, and complete separation attained, in a finite amount of time. For example, one implicit analytic solution to (54) can be obtained for $a = b = \frac{1}{2}$, i.e.,

$$t - t_o = 6(1 + 4\kappa)\arcsin(2\Phi_o - 1) + 12(4\kappa + 2\Phi_o - 1)\sqrt{\Phi_o(1 - \Phi_o)}. \quad (56)$$

In all calculations shown in this paper we assume $\kappa = 1$, in which case the time to go from $\Phi_o \approx 0$ to $\Phi_o = 1$ is $t_{\max} = 30\pi$.

Some sample curves of $t_{\max}$ (time for complete separation) versus a (with $b = a$) and Φ_o versus t are shown in Figure 2 for numerical solutions of (54). For a and b close to 1 separation starts gradually, accelerates, and then tapers off again toward completion. As a and b approach 0.4, this separation style is reversed; that is, separation is very rapid initially, tapering to a slower rate later, and accelerating again toward completion. This illustrates the influence of the surface tension "pinching" effect when the magnitude of the interface curvature reaches infinity as ϕ approaches 0 or 1. As a and b approach 0, the surface tension force weakens and separation becomes slower.

4.3.2. Numerical experiments. We next examine solutions of (30) and (42) using basic second order finite differences, with a tridiagonal matrix solution for the finite difference version of (42), and an explicit time integration (with a time step constrained to be $\leq 10^{-2}$ of the Courant time step) for (30). Solutions are tested on various finite difference grids which have between 101 and 501 points; we find that 201 grid points are sufficient to satisfy convergence tests.

The medium is of finite width ($-100 \leq y \leq +100$), and the boundary conditions are, again, that $w = 0$ at $y = \pm 100$. We assume that ϕ obeys (30) at the boundaries as well as in the interior (since ϕ has no boundary constraints of its own). For all cases we keep $\lambda \ll 1$ (actually, 10^{-20}); numerical solutions to the self-separation problem with finite λ are discussed by RBS2. Finally, as with all other calculations in this paper we prescribe $\kappa = 1$. We investigate only a select number of solutions to illustrate the basic effect of varying a (for all cases we keep $b = a$). All solutions are initiated with a single long-wavelength perturbation

$$\phi(t{=}0) = 0.05 + 0.001\cos(\pi y/100). \quad (57)$$

Numerical solutions show the fluid concentrating toward the centerline $y = 0$ (Figure 3), although this tendency is dictated by the simple initial condition (57). The effect of decreasing a from 1 is to cause a more rapid draining of fluid away from the wall regions (because of the surface tension pinching effect), and thus a sharper slope along the flanks of the porosity anomaly along with a flatter maximum (Figures 3a and 3b). However, the time for $\phi_{\max} = \max(\phi)$ to reach values of order 1 (Figure 3c) is shortest for some intermediate value of a between 0 and 1, as predicted by the amplitude analysis (see Figure 2). The function $\phi_{\max}(t)$ also changes

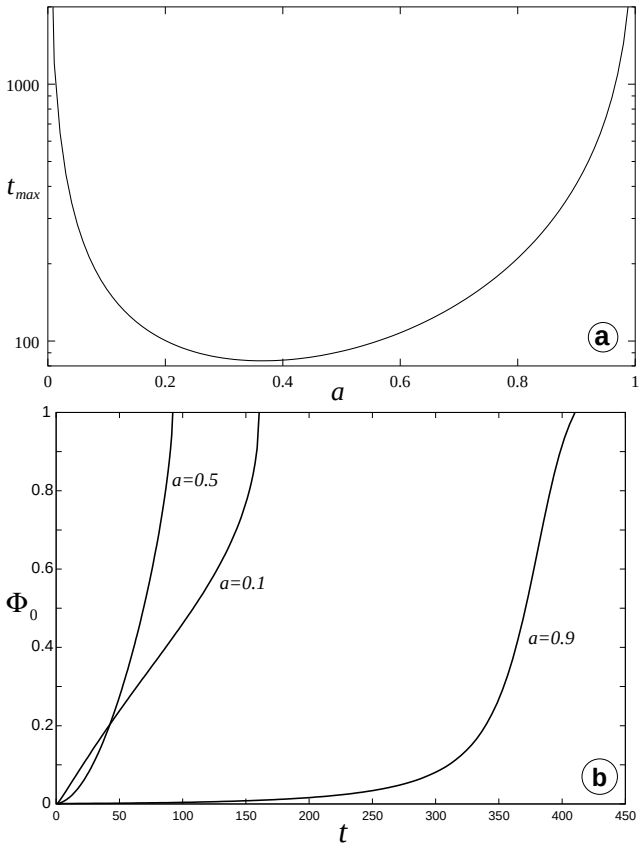

Figure 2. (a) Time for total separation of phases $t_{\max}$ versus a; and (b) peak porosity Φ_o versus time t for select values of a for the amplitude analysis of the surface tension driven self-separation. For all cases, $b = a$ and $\kappa = 1$, and we use an initial condition $\Phi_o = 10^{-3}$.

curvature with decreasing a (i.e., as a decreases the surface tension pinching effect causes more rapid separation when ϕ is near 0 and 1) as predicted by the amplitude analysis (compare Figure 3c with Figure 2b, noting that the times are not the same because of different initial conditions).

5. Damage and Shear Localization

We next consider shear localization and the influence of damage, or viscous deformational work on the interface, by allowing for $f\Psi' > 0$. In this case, the relevant equations are (30)-(33) subject to the boundary conditions (40).

5.1. Specific Equations

As noted by BRS1, the partitioning fraction f is unlikely to be constant. We can deduce one of the most basic dependences of f on the state of the system by considering the interface work equation (33), and the case of $\partial\phi/\partial t = 0$ which can occur in three instances: when $\phi = 0$, when $\phi = 1$, and at the boundary between regions where the matrix is dilating and collapsing. When $\phi = 0$ or 1, there is no interface and thus (33) is irrelevant. When $\partial\phi/\partial t = 0$ in the boundary between dilation and collapse, ϕ is neither 0 nor 1 and

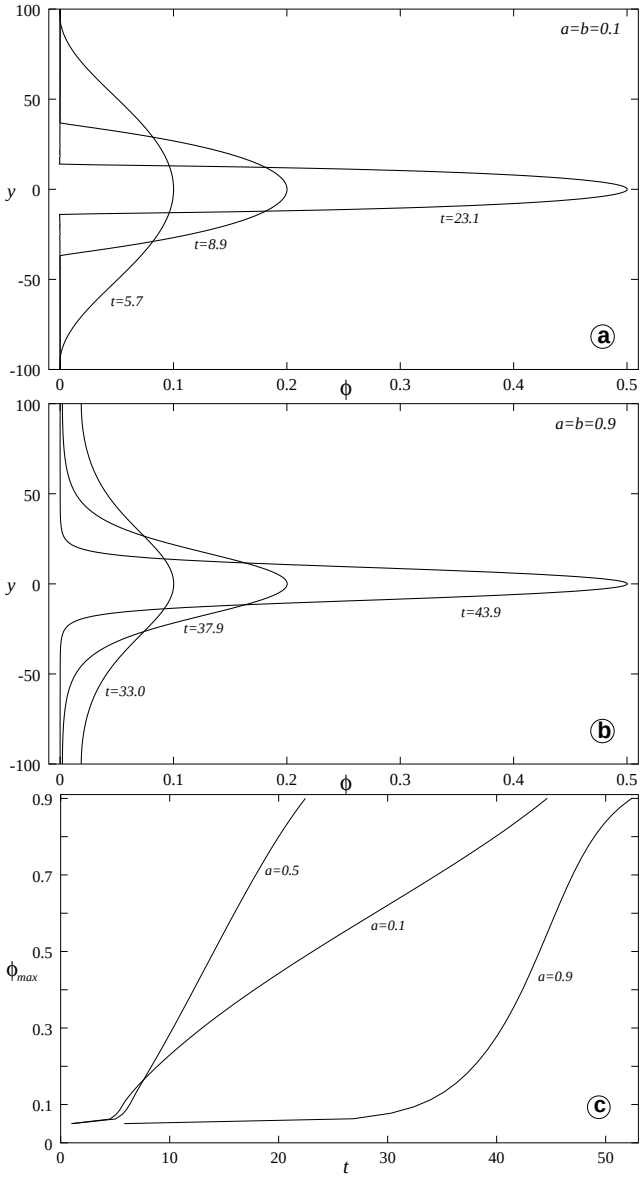

Figure 3. (a and b) Numerical experiments for two different values of a; and (c) time series of $\phi_{\max}$ for three different values of a. Values of a, b, and time t are indicated. In all cases, $b = a$, $\lambda = 0$, and $\kappa = 1$.

thus (33) applies. Moreover, in this case, $d\alpha'/d\phi$ is finite and we can thus safely assume that $\Delta\Pi$ is finite as well. In this boundary region the left-hand side of (33) is therefore 0, which dictates that $f\Psi' = 0$ as well. However, since $\Psi' > 0$ when shear is imposed (regardless of ϕ), the condition that $f\Psi' = 0$ can only be satisfied if $f = 0$ when $\partial\phi/\partial t = 0$.

The exact dependence of f on $\partial\phi/\partial t$ cannot be inferred from theory alone. However, we can use known constraints on f to estimate a simple form of this dependence; in particular, (1) f is positive definite and bound between 0 and 1; (2) f is invariant to a switch of ϕ and $1-\phi$ (see BRS1 for discussion of symmetry requirements); and (3) as indicated above, $f = 0$ when $\partial\phi/\partial t = 0$. Thus, if f is to be nonzero at all, it must increase from its value of 0 at $\partial\phi/\partial t = 0$ as $|\partial\phi/\partial t|$ increases. However, we cannot arbitrarily assume an unusual functional form for f, for example, a form where f equals zero or reaches an extremum at some value of $\partial\phi/\partial t$ other than $\partial\phi/\partial t = 0$. Thus, given the above constraints, we assume that f increases monotonically with $(\partial\phi/\partial t)^2$ (or some other even power of $\partial\phi/\partial t$ which are all positive definite and invariant to a switch of ϕ and $1-\phi$), while being bound between 0 and 1. We therefore estimate a simple monotonic relation of the form

$$f = \frac{f^* \left(\frac{\partial\phi}{\partial t}\right)^2}{\gamma + \left(\frac{\partial\phi}{\partial t}\right)^2}\ , \tag{58}$$

where $f^* \leq 1$ and is the maximum possible value of f and γ is a constant that governs the value of $(\partial\phi/\partial t)^2$ at which f approaches f^*. Clearly, there are other functions that can satisfy the minimum requirements on f. However, they must all have similar form, while the rational function given by (58) is analytically simplest. Moreover, f certainly may depend on other parameters (e.g., temperature). However, such dependencies cannot be deduced from the above considerations and most likely need to be inferred empirically. Interestingly, however, forced-shear experiments on layers of granular media have demonstrated that the frictional resistance (related to deformational work absorbed by the system) does indeed increase with total dilation rate rather than dilation itself, where the total dilation rate is related to the across-layer integral of $\partial\phi/\partial t$ [*Géminard et al.*, 1999].

With the adoption of (58), we can rewrite (33) in the tractable form

$$\Delta\Pi = -\frac{d\alpha'}{d\phi} - \frac{\kappa}{\phi(1-\phi)}\frac{\partial\phi}{\partial t} + \frac{f^*\frac{\partial\phi}{\partial t}}{\gamma + \left(\frac{\partial\phi}{\partial t}\right)^2}\Psi'. \tag{59}$$

Note that in limit of static equilibrium $\partial\phi/\partial t \to 0$, (59) recovers the equilibrium surface tension condition $\Delta\Pi = -d\alpha'/d\phi$ (see BRS1 and RBS2). For a constant σ the arguments leading to (58) and (59) can be generalized to three dimensions, in which case one would substitute $\overline{D}\phi/Dt$ for $\partial\phi/\partial t$ in these equations. In the end, our governing equations for one-dimensional damage and shear are (30)–(32) and (59).

5.2. Linear Stability Analysis

Again we examine the stability of a finite layer (with $-100 \leq y \leq +100$) of constant porosity undergoing shear and assume that $\phi = \phi_0 + \epsilon\phi_1$, $w = \epsilon w_1$, and $u = u_0 + \epsilon u_1$, where $\epsilon \ll 1$. The only equation that has an $O(\epsilon^0)$ contribution is the x component of the matrix force balance (31), which, with the boundary condition that $u = \pm U$ at $y = \pm 100$ leads to $u_o = \Omega y$, where $\Omega = U/100$, and we require that the perturbation $u_1 = 0$ at the boundaries. The equations that are $O(\epsilon^1)$ are the linearized mass conservation equation (44), which is unchanged from the self-separation

stability problem, and two linearized force balance equations

$$0 = (1-\phi_0)\frac{\partial^2 u_1}{\partial y^2} - \Omega\frac{\partial \phi_1}{\partial y} \tag{60}$$

$$0 = -G_0\frac{\partial \phi_1}{\partial y} - \nu\phi_0^2(1-\phi_0)\frac{\partial^2\phi_1}{\partial t\partial y} + \phi_0(\kappa+\phi_0)(1-\phi_0)^2\frac{\partial^2 w_1}{\partial y^2} - \lambda(1-\phi_0)w_1, \tag{61}$$

where (61) results after substitution of (59) into (32), $G_0 = G(\phi_0)$, and

$$\nu = \frac{3}{4}\frac{f^*}{\gamma}(1-\phi_0)^2\Omega^2. \tag{62}$$

Equation (60) only governs how u_1 is influenced by ϕ_1 but does not affect growth of porosity and therefore does not warrant a solution. We again assume that ϕ_1 and $w_1 \sim e^{iky+st}$, which leads to the dispersion relation

$$s = \frac{G_0k^2}{[\kappa+\phi_0(1-\nu)]\phi_0(1-\phi_0)k^2+\lambda}\ . \tag{63}$$

Thus shear and damage clearly accelerate the growth rate of the instability;for example, for cases in which $\lambda \ll 1$, the growth rate goes as $[\kappa+\phi_0(1-\nu)]^{-1}$, which approaches infinity as $\nu \to 1+\kappa/\phi_0$.

If ν exceeds $1+\kappa/\phi_0$, it is possible that the growth rate can become singular at

$$k = \sqrt{\lambda/[(\kappa+\phi_0[\nu-1])\phi_0(1-\phi_0)]} \tag{64}$$

and negative for larger wave numbers, in which case, the function $s(k)$ acts as a low-pass filter, that is, only modes with sufficiently small k (large wavelength) grow, while others decay. Interpretation of this effect will be deferred to discussion of the nonlinear numerical solutions (section 5.3.2).

5.3. Nonlinear Solutions

5.3.1. Amplitude analysis. As with the self-separation problem (section 4.3.1), we derive equations for the nonlinear evolution of a self-similarly shaped porosity anomaly in an infinite medium. For consistency, we use the same shapes for ϕ and w employed in the self-separation problem (i.e., (47) and (50), respectively), in which case the mass conservation equation (30) again leads to (51). As with the self-separation amplitude analysis (section 4.3.1), the domain is infinite ($-\infty \le y \le \infty$), and thus the relevant dimensional length scale is defined such that the half width δ of the porosity anomaly with amplitude Φ_o at any time t is $\delta(t) = 1/\Phi_o(t)$.

Although the layer has infinite width, we can only impose finite shear by insisting that $u = \pm U$ at some finite value of $y = \pm L'$. For consistency with the linear and numerical analyses we assign $L' = 100$. With these boundary conditions the equation governing velocity along the layer (31) has an analytical solution:

$$u = U\frac{y\sqrt{1-\Phi_0} + \arctan(y\Phi_0/\sqrt{1-\Phi_0})}{L'\sqrt{1-\Phi_0} + \arctan(L'\Phi_0/\sqrt{1-\Phi_0})}\ . \tag{65}$$

We eliminate $\Delta\Pi$ between (59) and (32) and then substitute (47), (50), and (65) into the resulting equation and (after taking $\partial/\partial y$ of this equation) evaluate it at $y = 0$ to obtain

$$0 = G(\Phi_0) - 12\Phi_0(\kappa+\Phi_0)(1-\Phi_0)^2W_0 + \frac{3f^*\Phi_0^2(1-\Phi_0)^4W_0}{(\gamma+\Phi_0^2(1-\Phi_0)^2W_0^2)^2} \cdot \left\{\frac{3}{4}\left[\gamma-\Phi_0^2(1-\Phi_0)^2W_0^2\right]\left(\frac{U}{\ell}\right)^2 + 8\Phi_0^2\left[\gamma+\Phi_0^2(1-\Phi_0)^2W_0^2\right]W_0^2\right\}, \tag{66}$$

where

$$\ell = L'(1-\Phi_0) + \sqrt{1-\Phi_0}\arctan(L'\Phi_0/\sqrt{1-\Phi_0}). \tag{67}$$

In deriving (66) we have assumed that since the shapes of ϕ and w are approximate, then factors of the form $N\psi_0 \pm M\psi(t)$ (where N and M are integer constants, ψ_0 is some constant, generally either 1 or γ, and $\psi(t)$ is some dependent variable, generally either Φ_0 or $d\Phi_0/dt$) are not significantly different from $N[\psi_0 \pm \psi(t)]$ or $\frac{1}{2}(N+M)[\psi_0 \pm \psi(t)]$ (depending on which yields simpler factors) as long as N and M are approximately equal (i.e., differ by no more than 33% from each other); for example, see section 4.3.1 in the discussion leading from (52) to (53). Equation (66) is a fifth order polynomial in W_0 which can be solved to yield the function $W_0(\Phi_0)$ (in fact, of the five possible roots, we choose the smallest, purely real, positive one such that (53) is recovered in the limit $f^* \to 0$). This function is then substituted into (51) to determine the nonlinear evolution and growth of Φ_0.

In fact, the exact evolution of Φ_0 with time differs little in appearance from that of the self-separation problem discussed in section 4.3.1 (see Figure 2). However, the timescale for separation and shear localization are affected significantly by shearing and damage. This timescale is again represented by the total time $t_{\max}$ for Φ_0 to go from 0 to 1, and we consider here how $t_{\max}$ is influenced by the parameters which represent shearing and damage (see Table 1), i.e., U, f^*, and γ (Figure 4).

When $U = 0$, all cases regardless of f^* have $t_{\max}$ very close to the pure self-separation $t_{\max}$ (with $f^* = 0$) which implies that damage has little effect without imposed shear. We refer to this self-separation $t_{\max}$ as t_{ss} which is only a function of a and b (see Figure 2a).

As $U \to \infty$ the leading term in (66) yields

$$\frac{3}{4}\left[\gamma-\Phi_0^2(1-\Phi_0)^2W_0^2\right]\left(\frac{U}{\ell}\right)^2 = 0, \tag{68}$$

which leads to the asymptotic solution

$$\frac{d\Phi_0}{dt} = \Phi_0(1-\Phi_0)W_0 \to \sqrt{\gamma} \tag{69}$$

independent of f^*; this yields an asymptotic $t_{\max} = 1/\sqrt{\gamma}$ (see Figure 4). Thus as U increases from 0, the separation

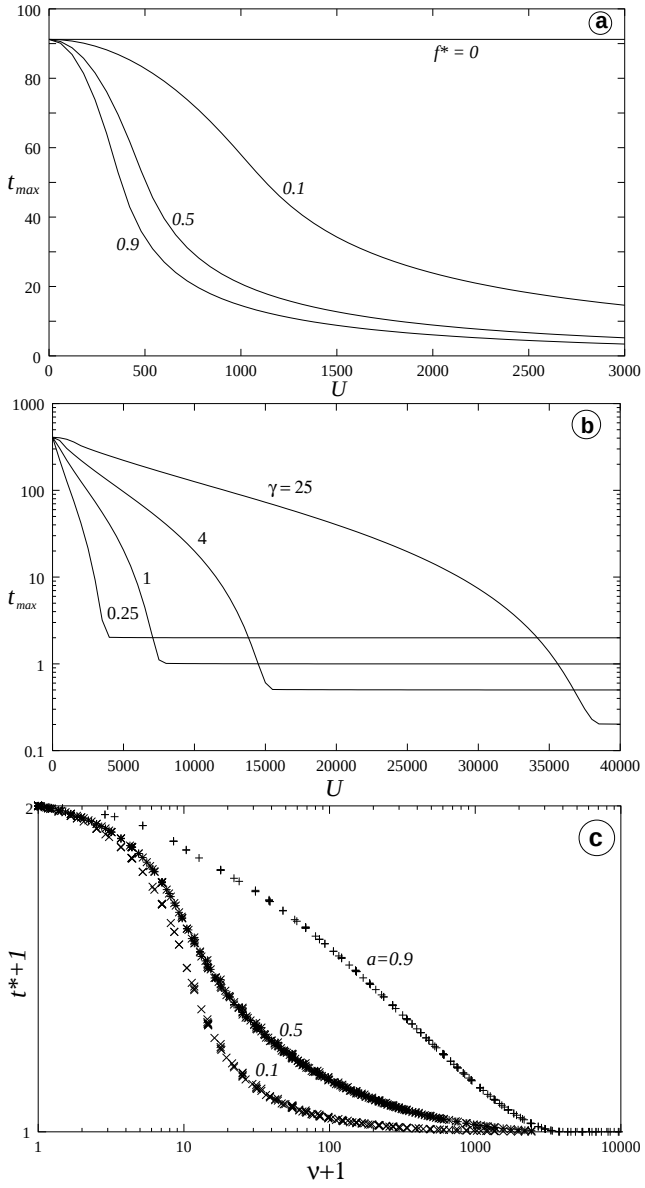

Figure 4. Time for complete separation of phases $t_{\max}$ versus shearing velocity U for (a) several different f^* (as indicated) with $a = b = 0.5$, and $\gamma = 1$ and (b) several different γ (indicated) with $a = b = f^* = 0.9$. (c) Total separation $t_{\max}$ versus shearing velocity U collapse to single curves that depend only on a (and b) when we plot $t^* = (\sqrt{\gamma}t_{\max} - 1)/(\sqrt{\gamma}t_{ss} - 1)$ versus ν (using (62) with $\phi_0 = 0$), where t_{ss} is the $t_{\max}$ for self-separation when $f^* = 0$ (see Figure 2). Also $t^* + 1$ and $\nu + 1$ are plotted in order to emphasize details on log-log axes. Curves for 27 cases are shown in Figure 4c: for each a (and $b = a$) indicated, there are nine curves corresponding to all permutations of $\gamma = 0.25, 1, 4$ with $f^* = 0.1, 0.5, 0.9$. For all calculations, $\kappa = 1$, and the initial condition is $\Phi_o = 10^{-3}$.

time $t_{\max}$ goes from t_{ss} to $1/\sqrt{\gamma}$; given that the minimum t_{ss} is approximately 10^2 for $\kappa = 1$ (see Figure 2a), then as long as $\gamma > 10^{-4}$, an increase in damage and shear (i.e., an increase in U for $f^* > 0$) will cause a reduction in $t_{\max}$, i.e., an acceleration in the separation of phases.

The value of U at which $t_{\max}$ reaches the asymptotic value of $1/\sqrt{\gamma}$ depends on f^* as well as γ itself. An increase in f^* causes the $t_{\max}$ to reach its asymptotic value at smaller U, that is, increasing f^* enhances the influence of damage, thus allowing shear to be more effective at accelerating phase separation (Figure 4). While an increase in γ decreases the asymptotic value of $t_{\max}$ (i.e., allows for greater possible acceleration of phase separation), it also increases the value of U at which this $t_{\max}$ is attained (i.e., decreases the effectiveness of damage and shear).

The influence of damage on the rate of phase separation can be most succinctly summarized by noting that $t_{\max}$ versus U curves for different f^*, and γ (but with the same a and b) can be very nearly collapsed on to the same curve if we assume that

$$t_{\max} = \frac{1}{\sqrt{\gamma}} + \left(t_{ss}(a,b) - \frac{1}{\sqrt{\gamma}} \right) F(\nu, a, b) \qquad (70)$$

(Figure 4c). However, since the amplitude analysis assumes a single self-similar shape for ϕ that narrows with time, it cannot account for the low-pass filter effect of $\nu > 1 + \kappa/\phi_0$ predicted in the linear stability analysis. Overall, the amplitude analysis predicts a considerable acceleration of phase separation by the addition of shear and damage.

5.3.2. Numerical experiments. We finally explore numerical solutions of (30)–(32) and (59), using, as with the self-separation problem, a finite difference scheme. As with the linear stability problem and previous numerical experiments, our dimensionless domain is $-100 \le y \le +100$. We employ the same initial and boundary conditions as stated in section 4.3.2, with the additional condition that $u = \pm U$ at $y = \pm 100$.

For simplicity, we do not fully explore all parameter space (which is, in fact, seven-dimensional, i.e., defined by a, b, U, γ, f^*, κ, and λ, not including initial conditions) and thus keep certain parameters fixed. As with all previous calculations, we set $\lambda \ll 1$, $\kappa = 1$, and $b = a$. In the end, the parameter space we explore is four-dimensional, over a, f^*, U, and γ; however, it is often more convenient to refer to ν instead of U (using $\phi_0 = 0.05$ in (62); also see Table 1).

The numerical solutions reveal three basic regimes which essentially depend only on ν, as displayed in Figure 5. These regimes are as follows:

1. For "low" values of ν ($\nu \le 2$) the porosity field collapses essentially in the same manner as the surface tension driven self-separation problem (see Figure 3). Only the growth rate of $\phi_{\max}$, the peak porosity value, appears to be affected by changes in U (or ν), f^*, and γ, as predicted by the stability and amplitude analyses (Figure 6). Thus, in this regime, changes in the shear and damage parameters U, f^*, and γ that cause an increase in ν induce only an acceleration of the self-separation effect. We refer to this regime as the "accelerated separation" regime of solutions. As ν exceeds 1 and approaches 2, the porosity profile gradually displays

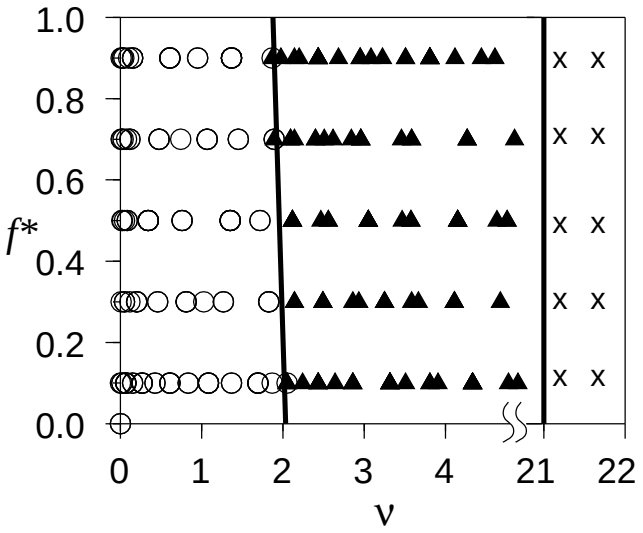

Figure 5. Regime diagram of the different types of numerical solutions of the 1-D flow problem with shear and damage. Three different types of solutions exist depending essentially only on the value ν. The regimes of solutions in ν-f^* parameter space separated by solid lines are shown. Symbols show the location in parameter space at which solutions were found. Circles indicate simple accelerated self-separation, solid triangles indicate solutions experiencing the tear localization, and crosses indicate solutions undergoing inhibition of phase separation or distributed damage. The diagram displays 243 solutions that have various permutations of $a = 0.1, 0.5, 0.9$ and $\gamma = 0.25, 1, 25$ over the ranges $0 \leq f^* \leq 0.9$ and $0 \leq U \leq 2000$. See section 5.3.2 for further discussion.

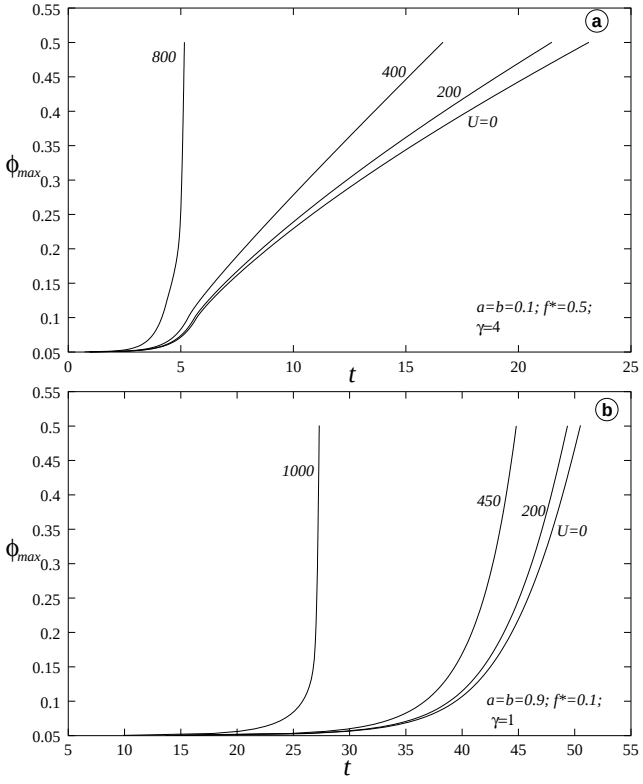

Figure 6. (a and b) Maximum porosity $\phi_{\max}$ versus time t for different values of U as labeled for two different sets of parameters indicated in the lower right corners of each frame. Exceptional growth rates associated with the tear localization occur at $U = 800$ in Figure 6a and $U = 1000$ in Figure 6b.

increased sharpening, leading to the regime discussed next.

2. For intermediate values of ν (i.e., $2 < \nu < 1+\kappa/\phi_0 = 21$ given $\kappa = 1$ and $\phi_0 = 0.05$) the porosity field undergoes a severe morphological change after some finite time. In particular, profiles of ϕ become concave above and below the centerline of $y = 0$, developing cusps or sharp peaks (Figure 7); soon after this sharpened peak forms the growth of $\phi_{\max}$ accelerates dramatically (Figure 6). At a certain point the peak becomes so sharp and the growth rates so steep that further numerical solutions are untenable; that is, the solution becomes numerically unstable as it appears to approach a singularity. We refer to this effect as a "tear localization," which is predicted by neither the linear stability nor amplitude analyses. As ν exceeds 5, the narrow tear localization initiates sooner in the calculation, and as $\nu \to 1+\kappa/\phi_0 = 21$, the localization occurs almost immediately after the calculation commences and barely progresses before approaching a singularity and thus ending the calculation.

3. When $\nu > 1 + \kappa/\phi_0$ (again, $1 + \kappa/\phi_0 = 21$ in these cases), the separation and concentration of fluid into a narrow zone are precluded; the initial porosity anomaly undergoes some slight initial collapse to a square-shaped profile (Figure 8) and then ceases any further evolution. This effect correlates with the exclusion of small wavelength (high wave number) instabilities (i.e., the low-pass filter effect) predicted by the linear stability analysis (section 5.2); that is, for $\nu > 1 + \kappa/\phi_0$ the porosity anomaly cannot collapse to less than a certain width (or wavelength). For cases of $\lambda \approx 0$ this minimum width is extremely large, thus effectively precluding significant collapse. We interpret the regime $\nu > 1 + \kappa/\phi_0$ as a state wherein shear and damage overwhelm surface tension driven self-separation and cause void generation and growth throughout the layer, over large wavelengths and thus nearly uniformly. In other words, when $\nu > 1 + \kappa/\phi_0$, damage is so effective that instead of causing shear localization it effectively induces microcracking throughout the layer. We refer to this regime as the "distributed damage" regime (Figure 5).

6. Discussion and Conclusion

6.1. Summary

A two-phase model that accounts for both surface tension and viscous deformational work on the interface between phases has been used to examine damage and shear localization. Even without shear and damage, the two vis-

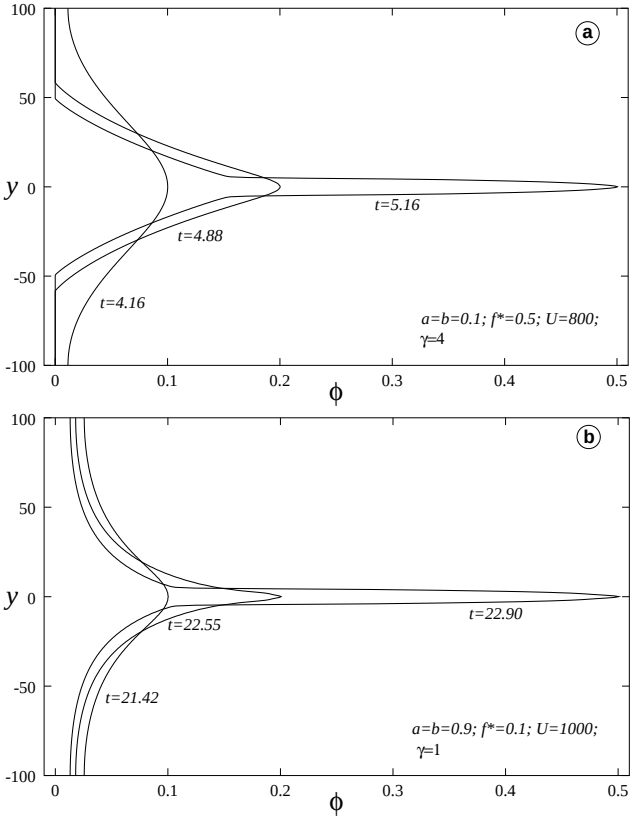

Figure 7. Porosity fields at different times (as indicated) to illustrate the onset of the tear localization for different parameter values (indicated in the lower right corner of each frame). These solutions can be compared to those of Figures 3a and 3b which use the same values of a and b as shown here, but without shear and damage. Growth of the peak porosity for the cases above are shown in Figure 6.

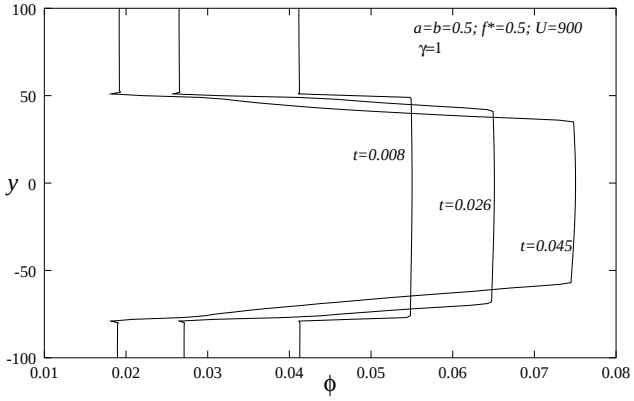

Figure 8. Porosity fields at different times (as indicated) to illustrate the distributed damage regime when $\nu > 1 + \kappa/\phi_0$ which for the given parameter set means $\nu > 21$. With the parameters of the above calculation (indicated in the top right corner) $\nu = 27.4$. The porosity field undergoes only slight collapse from a nearly constant value of $\phi = 0.05$ to an anomaly with peak porosity $\phi = 0.075$, after which the field ceases evolution and the calculation goes numerically unstable. Even during this slight collapse the porosity field assumes a broadened square shape, indicating the exclusion of small-wavelength features (i.e., no narrow or even rounded peaks as in Figures 3 and 7).

cous phases would naturally separate due to gradients in surface tension. However, shear and damage can affect phase separation in a variety of ways; the main parameter controlling this behavior is ν, as defined in (62) (see also Table 1), which combines information about imposed shear velocity (or shear strain rate) with the damage partitioning (i.e., the fraction of deformational work stored on the interface as surface energy). The three basic behaviors or regimes arising from shear and damage are as follows:

1. For relatively small values of the parameter ν ($0 < \nu < 2$ for the cases shown in this study) the combination of shear and damage essentially only accelerates the natural self-separation.

2. With larger ν ($2 < \nu < 21$ for the parameters used here) shear and damage have a dramatic effect, in particular inducing a tear localization in which the porosity concentration becomes nearly singular in space and grows very rapidly.

3. Excessive amounts of shear and damage ($\nu > 21$ for this study) can inhibit the separation of phases, inducing uniform void or microcrack generation in lieu of focused and weak shear zones.

The theory and calculations presented here are still fairly idealized. Nevertheless, the three regimes listed above are suggestive of some basic behavior of failure and cracking (with the caveat that that the theory is based on viscous flow while brittle and brittle-ductile failure involves damage in elastic and plastic materials). For low stress and deformation rates, brittle and brittle-ductile materials are known to experience distributed microcracking which, especially with increased stress and deformation, leads to focusing of microcracks along narrow shear planes [*Lockner*, 1995; *Evans and Kohlstedt*, 1995; *Mathur et al.*, 1996; *Regenauer-Lieb*, 1998]. This behavior is suggested by the first two regimes presented here. The third regime of distributed void generation and inhibition of localization at high shear rates suggests that at a critical deformation rate, the damage around the shear localization can no longer accommodate the energy input by the imposed deformational work, thus leading to deposition of energy in the form of damage throughout the volume of the material. In terms of damage permeating the medium instead of becoming localized, this behavior is suggestive (again keeping in mind all the theory's inherent simplifications) of crack branching instabilities wherein at a critical crack speed smoothly propagating cracks give way to branching and extensive distributed damaging of the surrounding material and retardation of the original crack's propagation [*Boudet et al.*, 1995; *Sharon et al.*, 1995; *Marder and Fineberg*, 1996; *Fineberg and Marder*, 1999; *Adda-Bedia et al.*, 1999; *Sander and Ghaisas*, 1999].

6.2. Applications to Plate Boundary Formation

Given its underlying viscous-flow formalism, the present theory is clearly more applicable to long-timescale geodynamical processes than to fracture and earthquake mechanics. Indeed, one of our primary motivations for this study is understanding the generation of tectonic plates from a convecting mantle, in particular, the focusing of lithospheric weak zones into plate boundaries [see *Bercovici et al.*, 2000]. Thus, although the theory and model calculations presented are rather idealized, we will venture some speculation and evaluate the various model parameters as applicable to the Earth's lithosphere. In this case, we assume that the matrix is lithospheric silicate ($\mu_m \approx 10^{25}$ Pa s [*Beaumont*, 1976; *Watts et al.*, 1982]), while the fluid is water ($\mu_f \approx 10^{-3}$ Pa s [*Furbish*, 1997). The Darcy resistance parameter λ in this situation is negligibly small; that is, given that $c = \mu_f/k_o$ (where k_o is a reference permeability), we can choose the smallest possible $k_o \approx 10^{-10}\text{m}^2$ [*Spiegelman*, 1993a] and a maximum fluid zone width R of 1-10 km (typical of tectonic margin width) to obtain the largest likely λ of $\sim 10^{-10}$. Therefore the assumption that λ is negligible in many of the cases shown in this paper is valid for the case of lithospheric deformation. The values of both the dimensionless velocity U and time t depend on the quantity $\sigma\alpha_0$. One can estimate σ according to the values of surface tension in silicates [e.g., *Spry*, 1983; *Lasaga*, 1998; see BRS1 and RBS2] or from true fracture surface energy [*Atkinson and Meredith*, 1987], which indicate values of σ between 0.1 and 10 J m^{-2}; however, it is generally recognized that the effective surface energy of fractures is much higher, i.e., between 100 and 1000 J m^{-2} [*Jaeger and Cook*, 1979; *Atkinson*, 1987; *Atkinson and Meredith*, 1987]. The scale for α_0 is determined by grain size d and is typically of order of d^{-1} (see BRS1 and RBS2). With grains between 1 and 10 μm [*Spry*, 1983] we assume that representative values of $\sigma\alpha_0$ for fracture and microcracking range between 10^7 and 10^9 J m^{-3}, which are indeed of the same order as peak lithospheric strengths [*Kohlstedt et al.*, 1995]. Using tectonic velocities $1 \text{ cm yr}^{-1} \leq V_x \leq 10 \text{ cm yr}^{-1}$, and the values of R and μ_m already listed, we thus arrive at $10^2 \leq U \leq 10^6$.

In order to generate plate boundaries by shear localization our model lithosphere must have, according to our 1-D analysis, $\nu < 1 + \kappa/\phi_0$ (where κ is $O(1)$), and if the narrow tear localization is to play a role in boundary formation, then $\nu > O(1)$. These conditions can be met for a wide range of values of the maximum partitioning f^*, imposed shear velocity U, and other parameters contained in ν; that is, localization can occur at the upper end of the velocity range ($U = 10^6$) with little partitioning (a few fractions of a percent) and at the lower end of the velocity range ($U = 10^2$) with partitioning of the order of several tens of a percent. Where the range of plate tectonic velocities (which vary over only 1 order of magnitude) actually resides within the full range of $10^2 \leq U \leq 10^6$ is unclear, but it is apparent that localization can occur with plausible fractions of energy partitioning. (For comparison, laboratory experiments with metals show that partitioning of deformational work toward damage is typically 15-20% and maybe as much as 60% [*Chrysochoos and Martin*, 1989; *Chrysochoos et al.*, 1989, 1996].)

Finally, the minimum timescale, using $4\mu_m/(3\sigma\alpha_0)$, for lithospheric processes would be of the order of 100 Myr, which is also representative of the localization time in the model (i.e., the dimensionless time intervals for the shear localization calculations are of order 1-10; see Figure 6). Although this is a plausible timescale for slow tectonic processes (e.g., it is typical of a convective timescale), it is probably too large for plate boundary formation and certainly is too large to accommodate rapid boundary reorganizations. However, given the simplicity of both the theory and model calculations, obtaining timescales, velocities, and partitioning values that are tectonically and mechanically plausible is a positive step. Nevertheless, there is no doubt that further sophistication and realism must be incorporated into the theory before even moderately precise predictions can be ventured.

6.3. Future Directions

The two-phase model presented here offers a fundamental approach to treating damage; even with its simplifications, it predicts shear focusing, a narrow, nearly singular tear or crack-like localization, and even distributed damage and defocusing of microcracks suggestive of crack-branching instabilities. Nevertheless, the model has considerable room for improvement and sophistication, e.g., inclusion of anisotropy to account for organized interconnectedness of pores at low porosity; viscoelasticity to account for elastic storage of deformational energy; thermomechanical effects (e.g., thermal expansion of the fluid phase which affects pore pressure, thermoviscous behavior of matrix material, and temperature sensitivity of surface tension); phase changes and melting; phase reactions such as hydration and annealing, to name a few. Moreover, this study has been confined to one-dimensional calculations. Thus, even aside from further sophistication, future studies will use the theory to examine damage and localization in more complex geometries, such as in uniaxial compression, folding, slope failure, source sink driven models, buoyancy, and convectively driven flows. Invariably, the applications of the two-phase damage theory to numerous fields, such as granular dynamics, earthquake dynamics, structural geology, and generation of plate tectonics from mantle flow, are potentially endless.

Acknowledgments. This work benefited from discussions with Dan McKenzie and Rodey Batiza; helpful suggestions from George Bergantz, Craig Bina, and Klaus Regenauer-Lieb; and thoughtful reviews from Neil Ribe, Vladimir Lyakhovsky, and Ulrich Christensen. Support was provided by NSF (grant EAR-9458405), the Centre National de la Reserche Scientifique (CNRS), and NASA (HPCC grant NCCS5-147).

References

Adda-Bedia, M., R. Arias, M. Ben Amar, and F. Lund, Generalized Griffith criterion for dynamic fracture and the stability of crack motion at high velocities, *Phys. Rev. E, 60*, 2366–2376, 1999.

Ashby, M.F., and C.G. Sammis, The damage mechanics of brittle solids in compression, *Pure Appl. Geophys., 133*, 489–521, 1990.

Atkinson, B.K., Introduction to fracture mechanics and its geophysical applications, in *Fracture Mechanics of Rock*, edited by B.K. Atkinson, pp. 1–26, Academic, San Diego, Calif., 1987.

Atkinson, B.K., and P.G. Meredith, Experimental fracture mechanics data for rocks and minerals, in *Fracture Mechanics of Rock*, edited by B.K. Atkinson, pp. 427–525, Academic, San Diego, Calif., 1987.

Balachandar, S., D.A. Yuen, and D.M. Reuteler, Localization of toroidal motion and shear heating in 3-D high Rayleigh number convection with temperature-dependent viscosity, *Geophys. Res. Lett., 22*, 477-480, 1995.

Beaumont, C., The evolution of sedimentary basins on a viscoelastic lithosphere, *Geophys. J. R. Astron. Soc., 55* 471–497, 1976.

Bercovici, D., A simple model of plate generation from mantle flow, *Geophys. J. Int., 114*, 635–650, 1993.

Bercovici, D., A source-sink model of the generation of plate tectonics from non-Newtonian mantle flow, *J. Geophys. Res., 100*, 2013–2030, 1995a.

Bercovici, D., On the purpose of toroidal flow in a convecting mantle, *Geophys. Res. Lett., 22*, 3107–3110, 1995b.

Bercovici, D., Plate generation in a simple model of lithosphere-mantle flow with dynamic self-lubrication, *Earth Planet. Sci. Lett., 144*, 41–51, 1996.

Bercovici, D., Generation of plate tectonics from lithosphere-mantle flow and void-volatile self-lubrication, *Earth Planet. Sci. Lett., 154*, 139–151, 1998.

Bercovici, D., Y. Ricard, and M.A. Richards, The relation between mantle dynamics and plate tectonics: A primer, in *History and Dynamics of Global Plate Motions, Geophys. Monogr. Ser.*, vol.121, edited by M.A. Richards, R. Gordon and R. van der Hilst, pp. 5-46, AGU, Washington, D.C., 2000.

Bercovici, D., Y. Ricard, and G. Schubert, A two-phase model of compaction and damage, 1, General theory, *J. Geophys. Res.*, this issue.

Boudet, J.F., S. Ciliberto, and V. Steinberg, Experimental study of the instability of crack propagation in brittle materials, *Europhys. Lett., 30*, 337-342, 1995.

Chrysochoos, A., and G. Martin, Tensile test microcalorimetry for thermomechanical behaviour law analysis, *Mater. Sci. Eng., A108*, 25–32, 1989.

Chrysochoos, A., O. Maisonneuve, G. Martin, H. Caumon, and J.C. Chezeaux, Plastic and dissipated work and stored energy, *Nucl. Eng. Design, 114*, 323-333, 1989.

Chrysochoos, A., H. Pham and O. Maisonneuve, Energy balance of thermoelastic martensite transformation under stress, *Nucl. Eng. Design, 162*, 1–12, 1996.

Evans, B., and D.L. Kohlstedt, Rheology of rocks, in *Rock Physics and Phase Relations: A Handbook of Physical Constants, AGU Ref. Shelf* vol. 3, edited by T.J. Ahrens, pp. 148–165, AGU, Washington, D.C., 1995.

Fineberg, J., and M. Marder, Instability in dynamic fracture, *Physics Reports, 313*, 2–108, 1999.

Furbish, D.J., *Fluid Physics in Geology*, Oxford Univ. Press, New York, 1997.

Géminard, J.-C., W. Losert, and J.P. Gollub, Frictional mechanics of wet granular material, *Phys. Rev. E, 59*, 5881-5890, 1999.

Griffith, A.A., The phenomenon of rupture and flow in solids, *Philos. Trans. R. Soc. London, Ser. A, 221*, 163–198, 1921.

Gurnis, M., S. Zhong, and J. Toth, On the competing roles of fault reactivation and brittle failure in generating plate tectonics from mantle convection, *History and Dynamics of Global Plate Motions*, edited by M. Richards, R. Gordon, and R. van der Hilst, pp. 73-94, AGU, Washington, D.C., 2000.

Hansen, N.R., and H.L. Schreyer, Thermodynamically consistent theories for elastoplasticity coupled with damage, in *Damage Mechanics and Localization*, edited by J.W. Ju and K.C. Valanis, pp. 53–67, Am. Soc. Mech. Eng., New York, 1992.

Jaeger, J.C., and N.G.W. Cook, *Fundamentals of Rock Mechanics*, 3rd ed., Chapman and Hall, New York, 1979.

Jin, D., S.-I. Karato, and M. Obata, Mechanisms of shear localization in the continental lithosphere: Inference from the deformation microstructures of peridotites from the Ivrea zone, northwestern Italy, *J. Struct. Geol., 20*, 195–209, 1998.

Kameyama, M., D.A. Yuen and H. Fujimoto, The interaction of viscous heating with grain-size dependent rheology in the formation of localized slip zones, *Geophys. Res. Lett., 24*, 2523–2526, 1997.

Karato, S.-I., Grain growth kinetics in olivine aggregates, *Tectonophysics, 168*, 255–273, 1989.

Kohlstedt, D.L., B. Evans and S.J. Mackwell, Strength of the lithosphere: Constraints imposed by laboratory experiments, *J. Geophys. Res., 100*, 17,587–17,602, 1995.

Lasaga, A.C., *Kinetic Theory in the Earth Sciences*, Princeton Univ. Press, Princeton, N.J., 1998.

Lemaitre, J., *A Course on Damage Mechanics*, Springer-Verlag, New York, 1992.

Lemonds, J., and A. Needleman, Finite element analyses of shear localization in rate and temperature dependent solids, *Mech. Mater., 5*, 339–361, 1986.

Lockner, D.A., Rock failure, in *Rock Physics and Phase Relations: A Handbook of Physical Constants, AGU Ref. Shelf*, vol. 3, edited by T.J. Ahrens, pp. 127–147, AGU, Washington, D.C., 1995.

Lyakhovsky, V., Y. Ben-Zion, and A. Agnon, Distributed damage, faulting, and friction, *J. Geophys. Res., 102* 27,635–27,649, 1997.

Marder, M., and J. Fineberg, How things break, *Phys. Today, 49*(9), 24–29, 1996.

Marone, C., Laboratory-derived friction laws and their application to seismic faulting, *Annu. Rev. Earth Planet. Sci., 26*, 643–696, 1998.

Mathur, K.K., A. Needleman, and V. Tvergaard, Three dimensional analysis of dynamic ductile crack growth in a thin plate, *J. Mech. Phys. Solids, 44*, 439–464, 1996.

McKenzie, D., The generation and compaction of partially molten rock, *J. Petrol., 25*, 713–765, 1984.

Poirier, J.P., Shear localization and shear instability in materials in the ductile field, *J. Struct. Geol., 2*, 135–142, 1980.

Povirk, G.L., S.R. Nutt, and A. Needleman, Continuum modelling of residual stresses in metal-matrix composites, in *Residual Stress in Composites*, edited by B.V. Barrera and V. Dutta, pp. 3-23, TMS, New York, 1994.

Regenauer-Lieb, K., Dilatant plasticity applied to Alpine collision: Ductile void growth in the intraplate area beneath the Eifel volcanic field, *J. Geodyn., 27*, 1-21, 1998.

Ricard, Y., D. Bercovici, and G. Schubert, A two-phase model of

compaction and damage, 2, Applications to compaction, deformation, and the role of interfacial surface tension, *J. Geophys. Res.*, this issue.

Sander, L.M., and S.V. Ghaisas, Thermal noise and the branching threshold in brittle fracture, *Phys. Rev. Lett., 83*, 1994–1997, 1999.

Schubert, G., and D.L. Turcotte, One-dimensional model of shallow mantle convection, *J. Geophys. Res., 77*, 945–951, 1972.

Scott, D.R., Seismicity and stress rotation in a granular model of the brittle crust, *Nature, 381*, 592–595, 1996.

Segall, P., and J. R. Rice, Dilatancy, compaction, and slip instability of a fluid-infiltrated fault, *J. Geophys. Res., 100*, 22,155-22,171, 1995.

Sharon, E., S.P. Gross, and J. Fineberg, Local crack branching as a mechanism for instability in dynamic fracture, *Phys. Rev. Lett., 74*, 5096–5099, 1995.

Sleep, N.H., Ductile creep, compaction, and rate and state dependent friction within major faults, *J. Geophys. Res., 100*, 13,065–13,080, 1995.

Sleep, N.H., Application of a unified rate and state friction theory to the mechanics of fault zones with strain localization, *J. Geophys. Res., 102*, 2875–2895, 1997.

Spiegelman, M., Flow in deformable porous media, part 1, Simple analysis, *J. Fluid Mech., 247*, 17–38, 1993a.

Spiegelman, M., Flow in deformable porous media, part 2, Numerical analysis–The relationship between shock waves and solitary waves, *J. Fluid Mech., 247*, 39–63, 1993b.

Spiegelman, M., Physics of melt extraction: Theory, implications and applications, *Philos. Trans. R. Soc. London, Ser. A, 342*, 23–41, 1993c.

Spry, A., *Metamorphic Textures*, 353 pp., Pergamon, New York, 1983.

Tackley, P.J., Self-consistent generation of tectonic plates in three-dimensional mantle convection, *Earth Planet. Sci. Lett., 157*, 9-22, 1998.

Tackley, P.J., The quest for self-consistent generation of plate tectonics in mantle convection models, in *History and Dynamics of Global Plate Motions*, edited by M. Richards, R. Gordon and R. van der Hilst, pp. 47-72, AGU, Washington, D.C., 2000.

Taylor, G.I., and H. Quinney, The latent energy remaining in metal after cold working, *Proc. R. Soc. London, Ser. A, 143*, 307–326, 1934.

Thatcher, W., and P.C. England, Ductile shear zones beneath strike-slip faults: Implications for the thermomechanics of the San Andreas fault zone, *J. Geophys. Res., 103*, 891–905, 1998.

Watts, A.B., G.D. Karner, and M.S. Steckler, Lithosphere flexure and the evolution of sedimentary basins, *Philos. Trans. R. Soc. London, Ser. A, 305*, 249–281, 1982.

Yuen, D.A., and G. Schubert, The role of shear heating in the dynamics of large ice masses, *J. Glaciol., 24*, 195-212, 1979.

D. Bercovici, Department of Geology and Geophysics, Yale University, P.O. Box 208109, New Haven, CT 06520-8109. (david.bercovici@yale.edu)

Y. Ricard, Laboratoire des Sciences de la Terre, Ecole Normale Supérieure de Lyon, 46 allée d'Italie, F-69364 Lyon, Cedex 07, France. (ricard@ens-lyon.fr)

G. Schubert, Department of Earth and Space Sciences, University of California, Los Angeles, 595 Circle Drive East, Los Angeles, CA 90095-1567. (schubert@ucla.edu)

Received November 17, 1999; revised May 19, 2000; accepted October 30, 2000.

This preprint was prepared with AGU's LaTeX macros v5.01, with the extension package 'AGU++' by P. W. Daly, version 1.6b from 1999/08/19.